Supporting Information

Directional Crystallization of C8-BTBT-C8 Thin Films in a Temperature Gradient

Guillaume Schweicher,[a] Guangfeng Liu,[a*] Pierre Fastrés,[a] Roland Resel,[b] Mamatimin Abbas,[c] Guillaume Wantz[c] and Yves Henri Geerts[a,d]

a). Laboratoire de chimie des polymères, Faculté des Sciences, Université Libre de Bruxelles (ULB), CP 206/01, Boulevard du Triomphe, 1050, Brussels, Belgium
b). Institute of Solid State Physics, Graz University of Technology, Petersgasse 16, 8010 Graz, Austria.
c). Université de Bordeaux, IMS, CNRS, UMR-5218, Bordeaux INP, ENSCBP, 33405 Talence, France
d). International Solvay Institutes of Physics and Chemistry, ULB, CP 231, Boulevard du Triomphe, 1050 Brussels, Belgium

Table of contents

concentration of 20 mg.ml^{-1} but treated by different ∇T conditions.

Table S3: Surface roughness values (Ra), film thickness, FWHM, and the vertical crystallite size after the ∇*T* treatments of the C8-BTBT-C8 thin films **10 - 19** produced using the same spin-coating concentration of 20 mg.ml^{-1} but treated by different ∇*T* conditions.

Figure S6: sXRD pattern of the polycrystalline powder C8-BTBT-C8 recorded at room temperature including the indexation of the most specific reflections.

Figure S7: *s*XRD scans of the films **1-10**. Indexation of the specific reflections is included.

Figure S8: The intense diffraction peak at q_z around 4.34 nm^{-1} belongs to the 002 reflection of C8-BTBT-C8 in films **1-10**.

Figure S9: in-plane GIXD (2θχ/ϕ scan) patterns of films **5** and **10** were recorded at room temperature.

Figure S10: *s*XRD scans of samples **5** and **11 - 19** produced using the same spin-coating concentration of 20 mg.ml^{-1} before (No.**5**) and after ∇*T* treatments (No.**11** - No.**19**).

Figure S11: (a) Low angular range *s*XRD curves of C8-BTBT-C8 spin-coated thin films **10-19**. (b) Evolution of the film thickness as a function of the pulling rate (V_p) for two Th - Tc

couples. All data were obtained at room temperature.

Figure S12: The diffraction peak in films 5, and 10-19 at q_z around 4.34 nm^{-1} belongs to the 002 reflection of C8-BTBT-C8.

Figure S13: Schematic representation of the pole figure measurement geometry.

Figure S14: Pole figure measurements of the C8-BTBT-C8 films **10-19** based on {113} reflections. The black solid dot highlights the temperature gradient direction.

1) Calibration of thermal gradient setup

A calibration of the magnitude of the selected ∇T setup was needed. Since uncertainties related to heat transfer at the glass to glass and glass to metal interfaces can result in the real magnitude of the gradient (G_{exp}) being smaller than G, which is directly calculated by the equation as $G = (T_h - T_c)/x$, where x = 2.0 mm is the gap between the hot and cold stages. Therefore, the method, mentioned in our previous report[S1] was used to calibrate the magnitude of G_{cal}, using C12-BTBT-C12. The latter was used instead of C8-BTBT-C8 because it allows to visualize both the melt-to-liquid crystal and the liquid-crystal-to-crystal boundaries, at 111.1 °C and 117.4°C, respectively. The T_h - T_c couples had to be adapted while preserving the same difference of temperature ΔT to ensure the visualization of both phase transition boundaries, as shown in Figure S2. Data are collected in Table S1 where d is the distance separating both phase transition fronts. The magnitude of ∇T effectively applied in alignment experiments of C8-BTBT-C8 (G_{exp}) is assumed to be very similar to G_{cal}, obtained with C12-BTBT-C12. This is a reasonable assumption because both compounds form similar SmA and crystalline phases.[s2]

Table S1. Calibration and experimental thermal gradient conditions.

Parameters	Calibration	Experiments	Calibration	Experiments
T_h (°C)	135	120	135	120
T_c (°C)	105	90	75	60

ΔT (°C)	30	30	60	60
d (mm)	1.04	-	0.59	-
Magnitude of ∇T (°C.mm^{-1})	$G_{cal} = 6.1$	$G_{exp} \approx 6$	$G_{cal} = 10.7$	$G_{exp} \approx 11$

S1 Panini, P.; Chattopadhyay, B.; Werzer, O.; Geerts, Y., Crystal Growth Alignment of β-Polymorph of Resorcinol in Thermal Gradient. *Cryst. Growth Des* **2018**, *18*, 2681-2689.

S2 Izawa, T.; Miyazaki, E.; Takimiya, K., Molecular Ordering of High-Performance Soluble Molecular Semiconductors and Re-evaluation of Their Field-Effect Transistor Characteristics. *Adv. Mater* **2008,** *20*, 3388-3392.

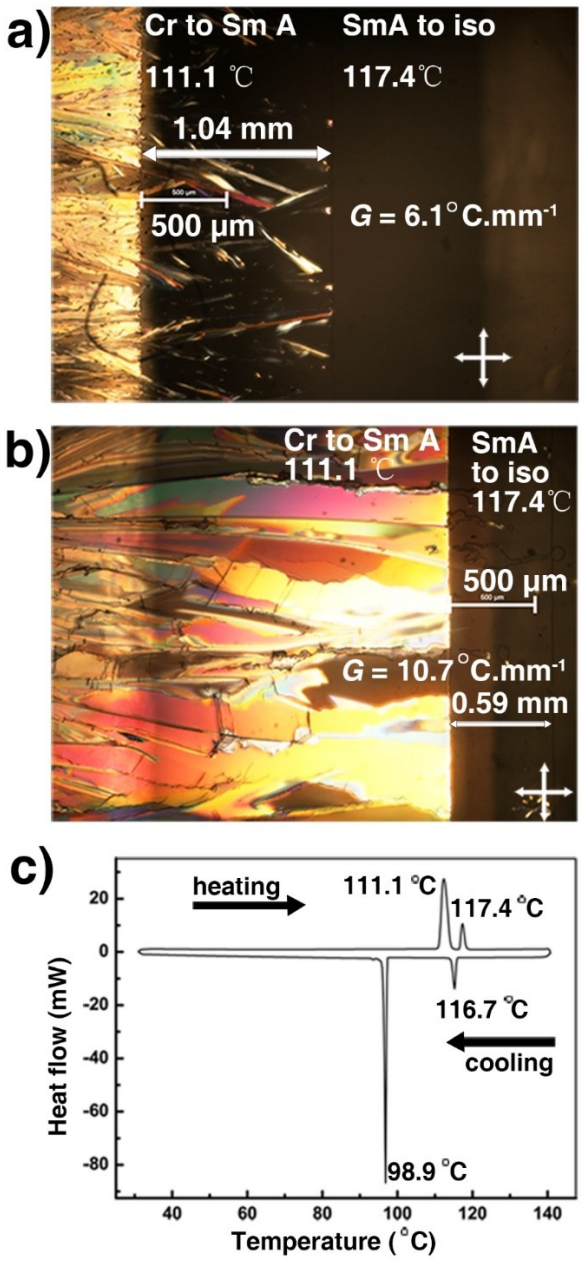

Figure S1. Calibration of 135 ℃ -105 ℃ T_h - T_c couple (a) and 135 ℃ -75 ℃ T_h - T_c couple (b), using the reference compound C12-BTBT-C12. Scale bar: 500 µm. (c) DSC data of compound C12-BTBT-C12.

3) Thermogravimetric analysis

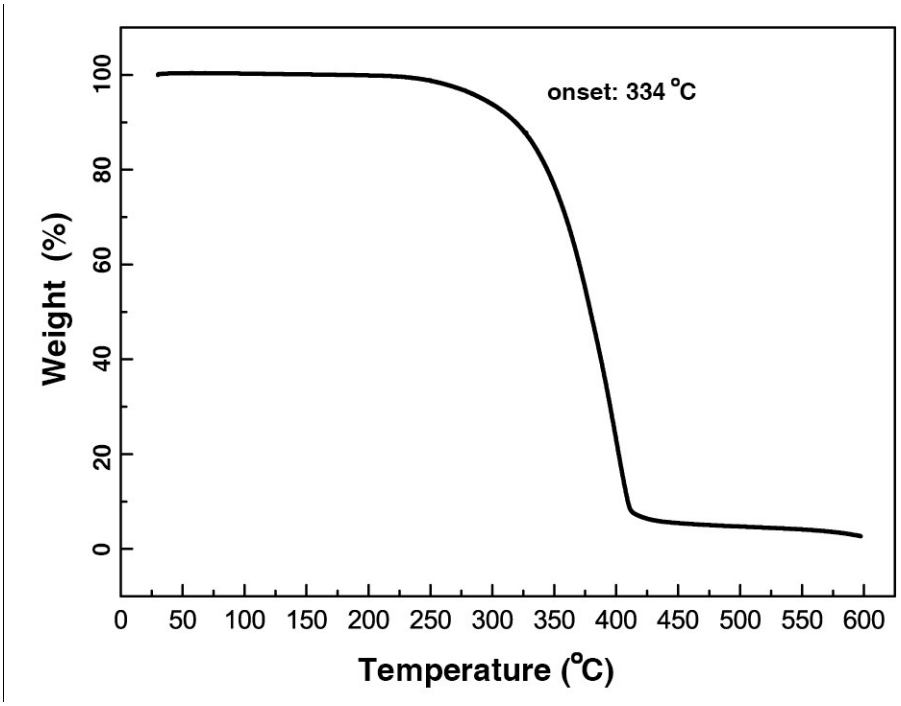

Figure S2. TGA trace of C8-BTBT-C8.

4) Surface morphology, roughness and thickness of thin films

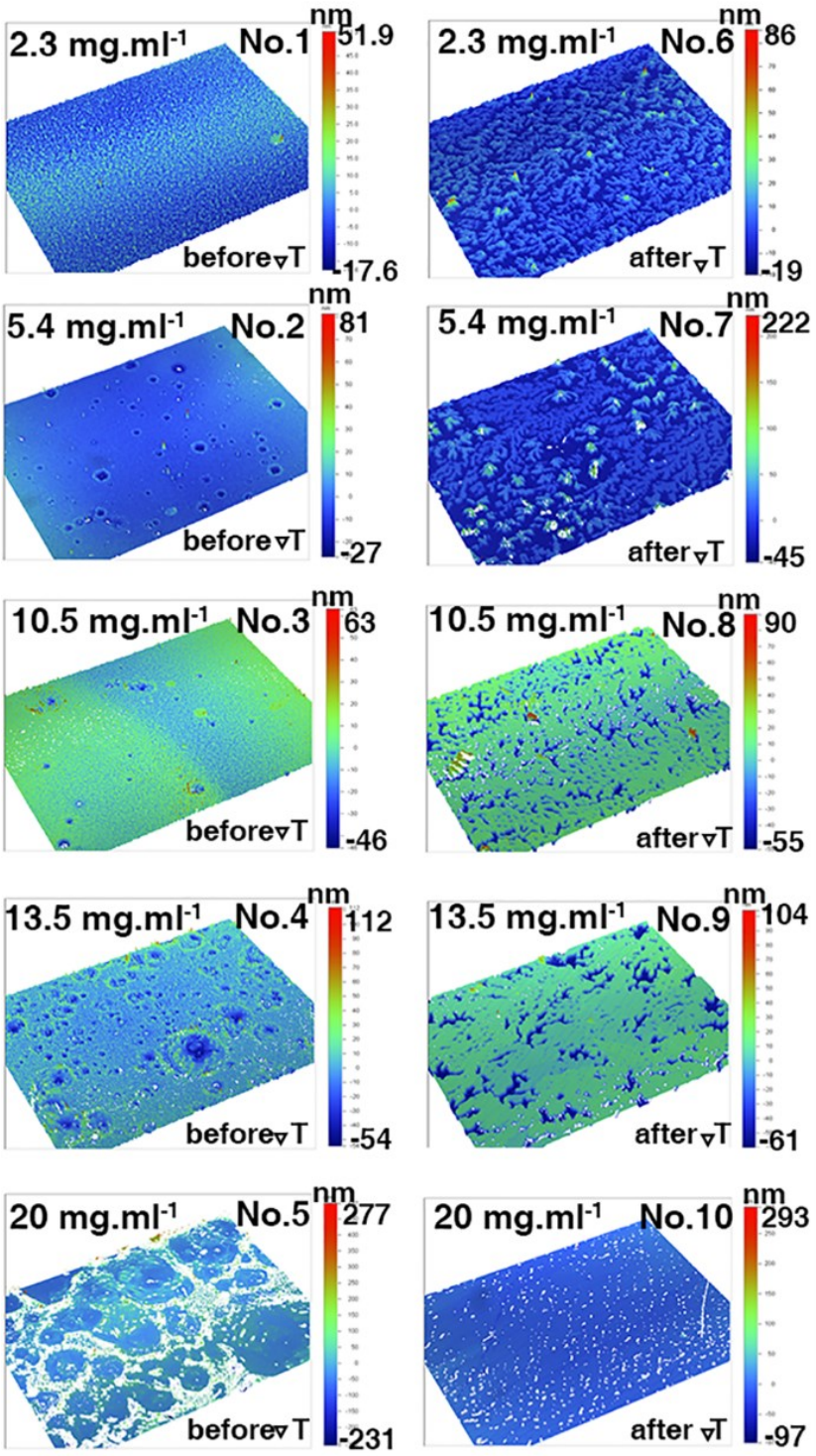

Figure S3. Optical profilometer 3D views of the C8-BTBT-C8 thin films produced using different spin-coating concentrations before (left images) and after (right images) the ∇T treatments (T_h - T_c couple: 120 °C - 90 °C; pulling rate V_p: 25 µm.s^{-1}).

Table S2. Surface roughness values (Ra), film thickness, FWHM (full width at half the

maximum of the diffraction peak, Δq), and crystallite size of the C8-BTBT-C8 thin films produced using different spin-coating concentrations before and after the ∇T treatments (T_h - T_c couple: 120 °C - 90 °C; pulling rate V_p: 25 μm.s^{-1}). Surface roughness values are extracted using optical profilometer images. Film thickness and FWHM data are extracted by *s*XRD measurements, respectively. Vertical crystallite size values are calculated by the Scherrer equation.

Sample (No.)	**Concentration (mg.ml^{-1})**	**Surface roughness values (Ra) (nm)**	**Film thickness (nm)**	**FWHM of (002), Δq (nm^{-1})**	**Vertical crystallite size (nm)**
1	2.3	4.71 (±0.560)	13.3 (±0.4)	0.954 (±0.043)	13.1 (±0.6)
2	5.4	4.30 (±0.010)	26.3 (±0.2)	0.484 (±0.027)	26.0 (±1.4)
3	10.5	5.470 (±0.010)	/	0.235 (±0.011)	53.7 (±2.5)
4	13.5	8.075 (±0.090)	/	0.184 (±0.006)	68.3 (±2.3)
5	20	25.96 (±2.890)	/	0.135 (±0.004)	92.7 (±3.1)
6	2.3	6.475 (±0.005)	25.9 (±0.9)	0.342 (±0.057)	36.2 (±6.6)
7	5.4	16.24 (±0.590)	42.3 (±0.2)	0.255 (±0.010)	49.4 (±1.9)
8	10.5	16.13 (±1.805)	69 (±1)	0.174 (±0.004)	72.6 (±1.7)
9	13.5	13.575 (±0.165)	84.3 (0.6)	0.160 (±0.004)	78.7 (±2.0)
10	20	5.465 (±0.025)	/	0.111 (±0.003)	113.4(±4.9)

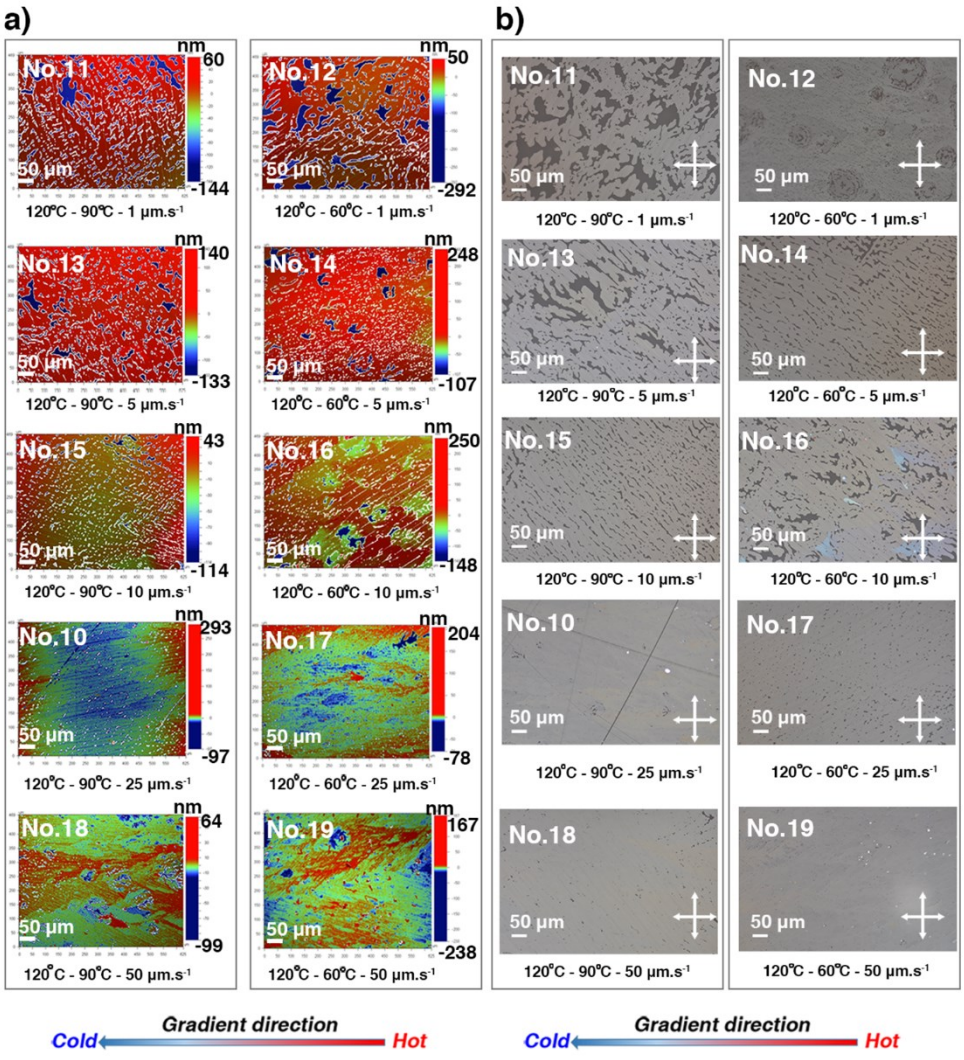

Figure S4. Surface morphology of the C8-BTBT-C8 spin-coated thin films **10-19**. (a) optical profilometry images; (b) POM images. Pictures were recorded at room temperature. The gradient direction is highlighted (bottom).

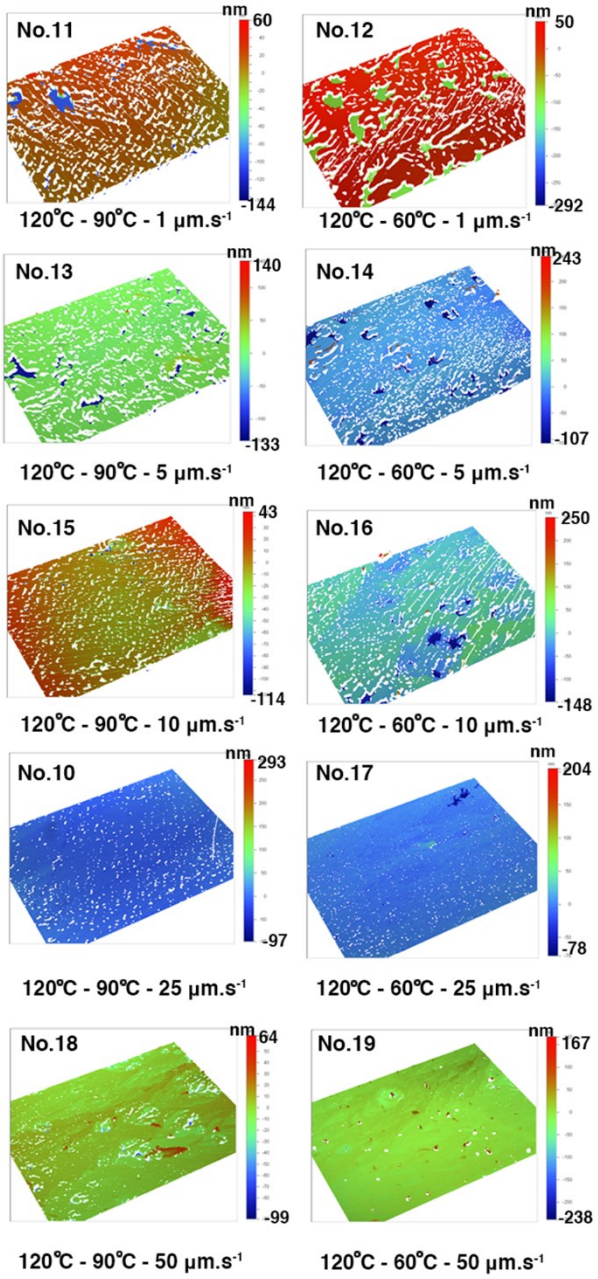

Figure S5. Optical profilometer 3D views of films **10 - 19** after the ∇T treatments. The films were produced using the same spin-coating concentration of 20 mg.ml^{-1} but were treated by different ∇T conditions.

Table S3. Surface roughness values (Ra), film thickness, FWHM, and crystallite size

after the ∇T treatments of the C8-BTBT-C8 thin films **10 - 19** produced using the same spin-coating concentration of 20 mg.ml^{-1} but treated by different ∇T conditions. Surface roughness values are extracted by optical profilometer images. Film thickness and FWHM data are extracted by *s*XRD (002) measurements, respectively. The vertical crystallite size values are calculated by the Scherrer equation.

Sample (No.)	**T_h (℃)**	**T_c (℃)**	**V_p (μm.s^{-1})**	**Thickness (nm)**	**Roughness Ra (nm)**	**FWHM of (002), Δq (nm^{-1})**	**Vertical crystallite size (nm)**
11	120	90	1	150 (±10)	24.365 (±0.255)	0.115 (±0.007)	109.1 (±6.8)
12	120	60	1	151 (±12)	26.3 (±1.460)	0.114 (±0.009)	111.0 (±8.6)
13	120	90	5	143 (±3)	18.68 (±0.100)	0.114 (±0.013)	110.7 (±12.2)
14	120	60	5	149 (±8)	14.12 (±1.180)	0.122 (±0.004)	103.1 (±3.9)
15	120	90	10	/	10.56 (±0.140)	0.104 (±0.003)	121 (±3.4)
16	120	60	10	134 (±2)	17.585 (±0.995)	0.120 (±0.009)	105.4 (±7.4)
10	120	90	25	/	5.465 (±0.025)	0.111 (±0.003)	113.4 (±4.9)
17	120	60	25	/	3.935 (±0.155)	0.117 (±0.003)	107.6 (±2.5)
18	120	90	50	/	4.62 (±0.140)	0.117 (±0.002)	107.7 (±2.2)
19	120	60	50	/	4.74 (±0.210)	0.125 (±0.002)	100.8 (±1.6)

5) X- ray measurements

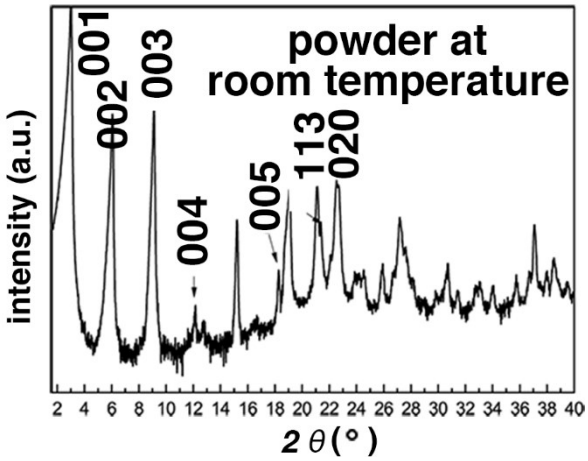

Figure S6. *s*XRD pattern of the polycrystalline powder of C8-BTBT-C8 recorded at room temperature. Indexation of the most specific reflections is included.

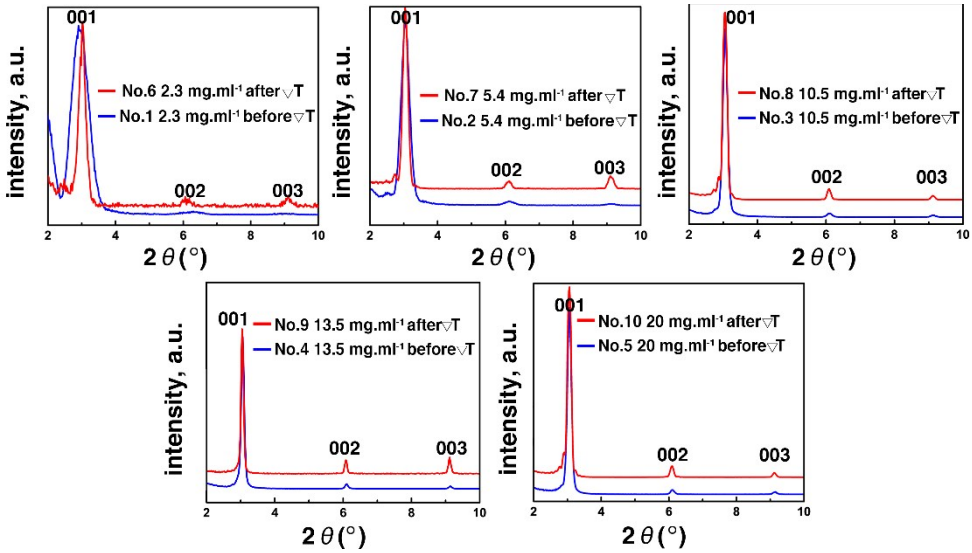

Figure S7. *s*XRD scans of the films **1-10**. Indexation of the specific reflections is included.

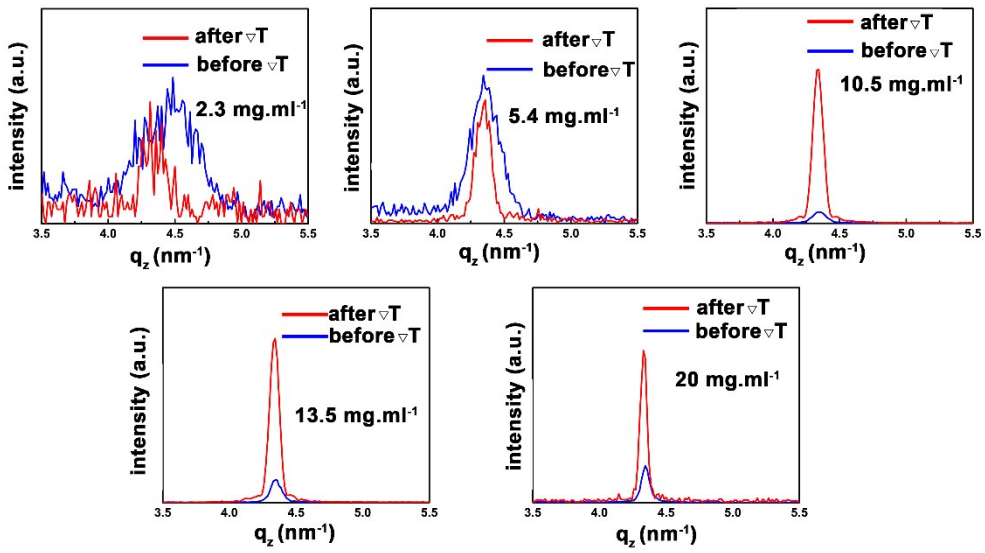

Figure S8. The intense diffraction peak at q_z around 4.34 nm^{-1} belongs to the 002 reflection of C8-BTBT-C8 in films **1**-**10**.

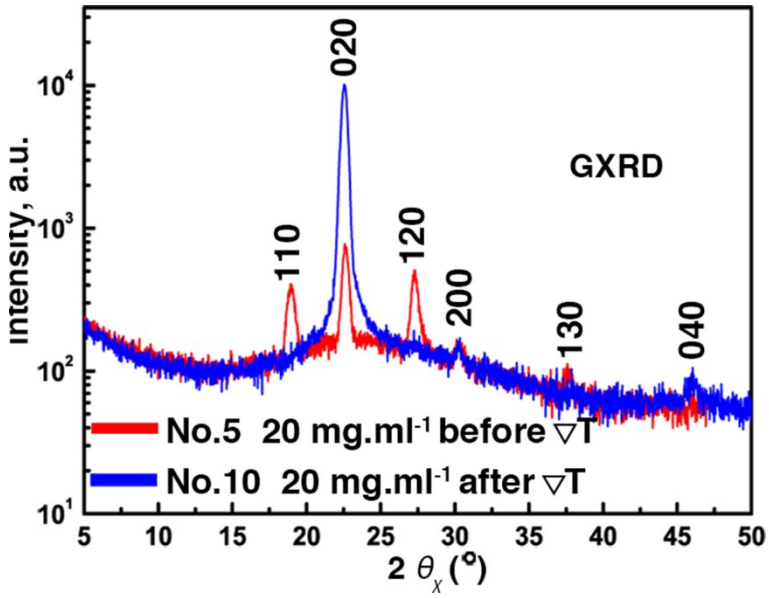

Figure S9. In-plane GIXD (2θχ/ϕ scan) patterns of films **5** and **10** recorded at room temperature.

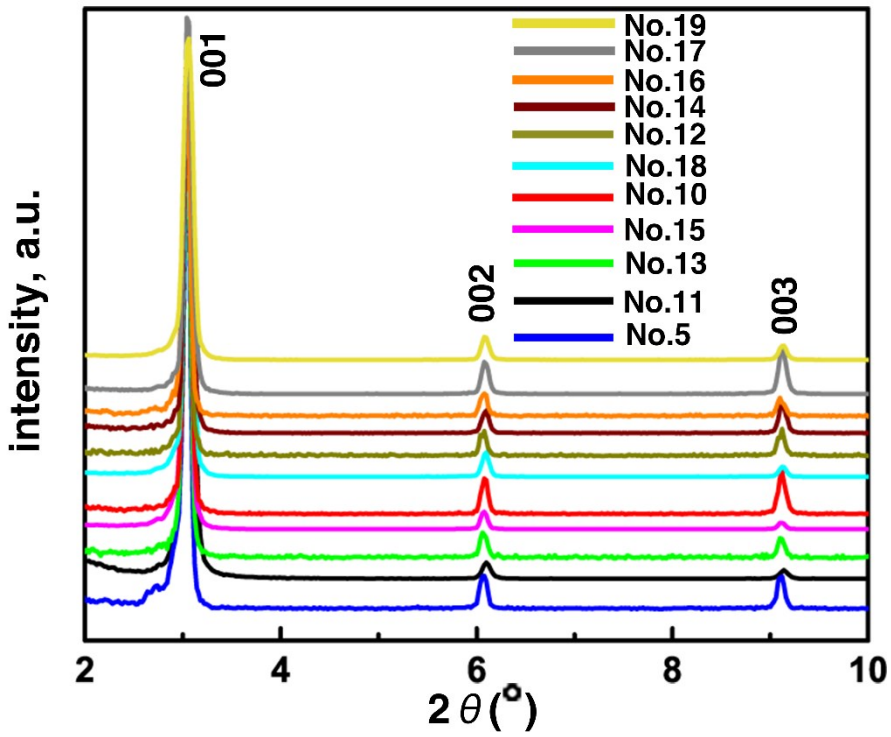

Figure S10. *s*XRD scans of samples **5** and **11 - 19** produced using the same spin-coating concentration of 20 mg.ml^{-1} before (No.**5**) and after ∇T treatments (No.**11** - No.**19**).

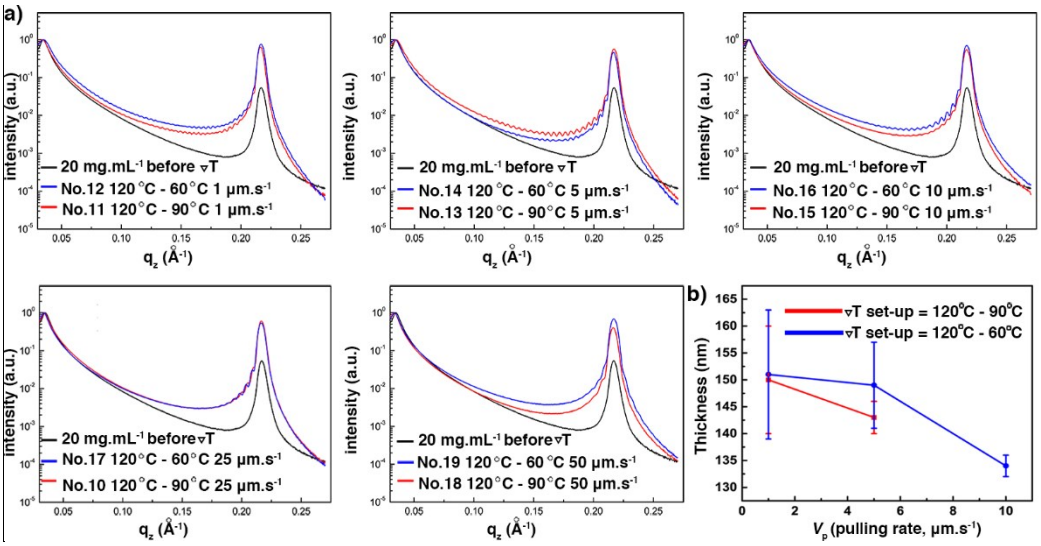

Figure S11. (a) Low angular range *s*XRD curves of C8-BTBT-C8 thin films **10-19**. (b) Evolution of the film thickness as a function of the pulling rate (V_p) for two T_h - T_c couples. All data were obtained at room temperature.

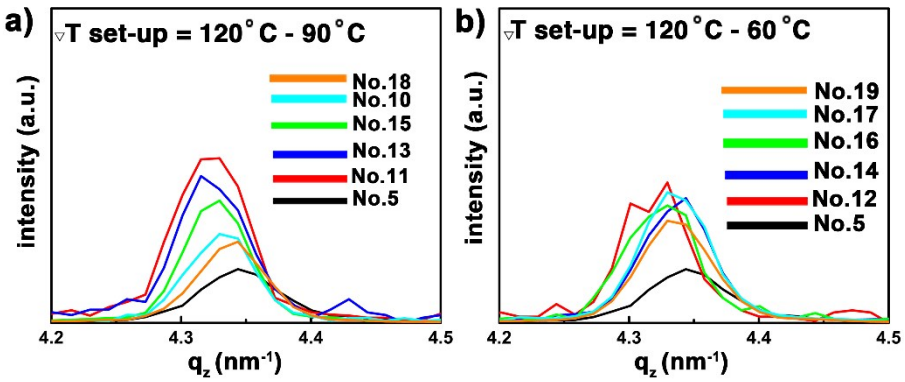

Figure S12. The diffraction peak in films 5, and 10-19 at q_z around 4.34 nm^{-1} belongs to the 002 reflection of C8-BTBT-C8.

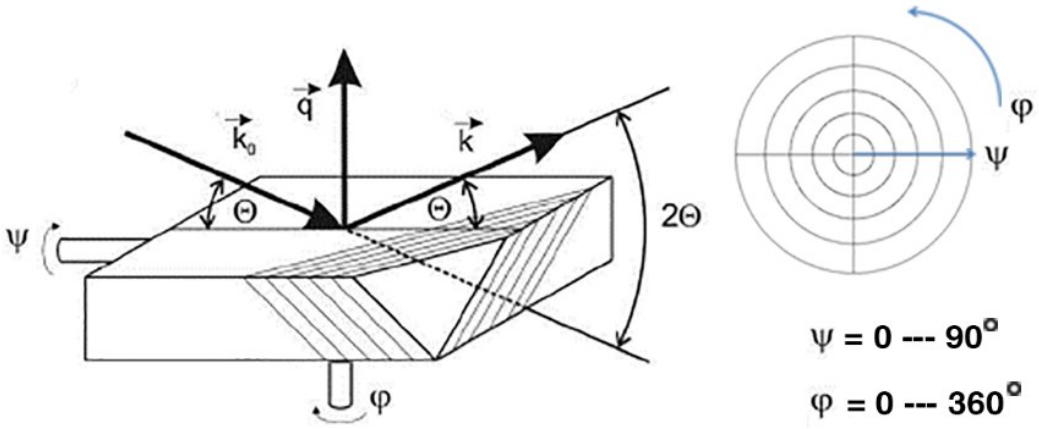

Figure S13. Schematic representation of the pole figure measurement geometry.

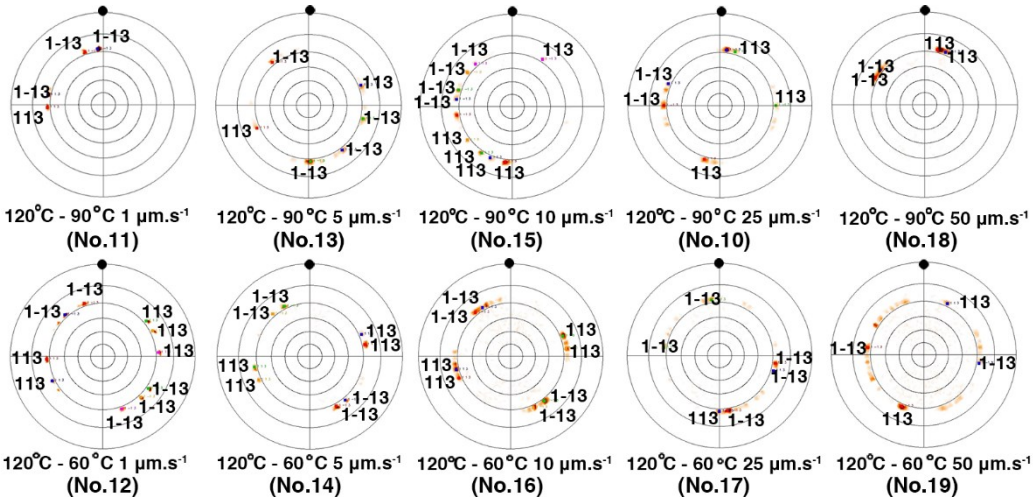

Figure S14. Pole figure measurements of the C8-BTBT-C8 films **10-19** based on {113} reflections. The black solid dot highlights the temperature gradient direction.